JOURNAL OF GEOPHYSICAL RESEARCH, VOL. 103, NO. D14, PAGES 17,099–17,110, JULY 27, 1998

Derivation of aerosol properties from satellite measurements of backscattered ultraviolet radiation: Theoretical basis

O. Torrcs,[1] P. K. Bhartia,[2] J. R. Herman,[2] Z. Ahmad,[3] and J. Gleason[2]

Abstract. We discuss the theoretical basis of a rccently developed technique to characterize aerosols from space. We show that the interaction between aerosols and the strong molecular scattering in the near ultraviolet produces spectral variations of the backscattered radiances that can be used to separate aerosol absorption from scattering effects. This capability allows identification of several aerosol types, ranging from nonabsorbing sulfates to highly UV-absorbing mineral dust, over both land and water surfaces. Two ways of using the information containcd in the near-UV radiances are discussed. In the first method, a residual quantity, which measures the departure of the observed spectral contrast from that of a molecular atmosphere, is computed. Since clouds yield nearly zero residues, this method is a useful way of separately mapping the spatial distribution of UV-absorbing and nonabsorbing particles. To convert the residue to optical depth, the aerosol type must be known. The second method is an inversion procedure that uses forward calculations of backscattered radiances for an cnscmble of aerosol models. Using a look-up table approach, a set of measurements given by the ratio of backscattered radiance at 340–380 nm and the 380 nm radiance are associated, within the domain of the candidate aerosol models, to values of optical depth and single-scattering albedo. No previous knowledge of aerosol type is required. We present a sensitivity analysis of various error sources contributing to the estimation of aerosol properties by the two methods.

1. Introduction

Aerosols affect the radiation budget of the Earth-atmosphere system directly by the scattering and absorption of solar and thermal radiation, and as cloud condensation nuclei, they also have an indirect effect by modifying the optical properties and lifetimes of clouds. The net effect on the radiative budget depends upon the aerosol composition and physical properties, the reflectivity of the underlying surface, and the altitude of the aerosol layers. Aerosol effects on the climate have been the focus of scientific interest for decades. The role of stratospheric aerosol of volcanic origin has traditionally received most of the attention (e.g., El Chichon and Mount Pinatubo eruptions), because of the large climate modification potential associated with the long lifetime of injected sulfate aerosols. Tropospheric aerosols, on the other hand, have only intermittently been the subject of research in the context of their potential climatic effects. In the last few years there has been a great deal of interest about the importance of the tropospheric aerosol load of anthropogenic origin such as industrial pollution and biomass burning.

The consequent aerosol effect on climate is usually quantified in terms of radiative forcing, i.e., the net flux change at the top of the atmosphere due solely to the direct aerosol radiative effects. Although there are uncertainties in the estimates of aerosol radiative forcing, it is generally agreed that the averaged global direct effects of anthropogenic sulfate aerosols are not negligible and are probably similar in magnitude but in opposite direction to anthropogenic greenhouse gas forcing [*Charlson et al.*, 1991]. Cooling effects from aerosols, however, do not nccessarily result in the cancelation of the greenhouse gases warming effect. Unlike the greenhouse gases, aerosol physical-chemical properties and abundances exhibit large variability in both time and space.

In addition to the well-documented cooling effect of aerosol particles by backscattering of shortwave radiation, some aerosol types also absorb solar radiation, reducing their cooling effect. For instance, absorption by both elemental and organic carbon aerosols from biomass burning and industrial pollution may affect the thermodynamics of the atmosphere by changing its thermal structure and perturbing convection and mixing processes in the planetary boundary layer. Silicaceous aerosols, such as desert dust, absorb solar and infrared radiation so that their direct effect on the climate may be significant. The role of anthropogenic sources of mineral aerosols as a climate-forcing factor has been examined [*Tegen et al.*, 1996] and found to be of importance when included in climate change studies. Because of thc lack of data on absorbing aerosol physical properties and their spatial and temporal distributions, the heating effects of aerosol particles may not have been adequately included in model calculations.

In spite of the difficulties inherent with satellite-based sensing, spaceborne measurements remain the most convenient method to characterize aerosol particles and determine their time and space distribution on a global basis. Currently available satellite data sets on aerosol properties do not providc a full description of the atmospheric aerosol load. The advanced very high resolution radiometer (AVHRR) aerosol data set provides information on optical depth only over the water surfaces of the Earth. The SAM and SAGE family of sensors were specifically designed to retrieve information on strato-

[1]Raytheon STX Corporation, Lanham, Maryland.
[2]NASA Goddard Space Flight Center, Greenbelt, Maryland.
[3]Science and Data Systems Inc., Silver Spring, Maryland.

Paper number 98JD00900.
0148-0227/98/98JD-00900$09.00

Table 1. Particle Size Distribution Parameters and Optical Properties of Aerosol Models Used in This Study

Aerosol Model	Parameters		Refractive Index	ω_0			τ		
	$r_0(\mu)$	σ		340	380	550	340	380	550
S1	0.07	2.03	1.43–0.000*i*	1.00	1.00	1.00	1.06	1.00	0.76
S2	0.40	1.43	1.43–0.000*i*	1.00	1.00	1.00	0.96	1.00	1.21
C1	0.14	1.45	1.55–0.020*i*	0.92	0.93	0.93	1.04	1.00	0.72
C2	0.14	1.45	1.55–0.040*i*	0.84	0.85	0.86	1.04	1.00	0.74
D1	0.07	1.95	1.57–0.015*i*	0.90	0.91	0.96	1.04	1.00	0.79
D2	0.25	2.20	1.57–0.015*i*	0.72	0.74	0.88	0.99	1.00	1.08
D3	0.50	2.20	1.57–0.015*i*	0.63	0.65	0.81	0.99	1.00	1.06

The values of ω_0 and τ (see text) at three wavelengths are listed. The 550 nm values are shown for comparison of the near UV with typical visible values.

spheric aerosols and do not function well in the lower troposphere. In addition, because of the nature of the solar occultation observing technique, both time and space coverage are very sparse. Several works have been recently published on the detection of absorbing aerosols using measurements of backscattered radiances in the near UV by the total ozone mapping spectrometer (TOMS). Using an uncalibrated aerosol index, the sources and geographic distribution of tropospheric absorbing particulate matter such as carbonaceous and mineral aerosols [*Hsu et al.*, 1996; *Herman et al.*, 1997] and ash aerosols from volcanic eruptions [*Seftor et al.*, 1997] have been described.

The choice of wavelengths for aerosol sensing from space has been traditionally driven by the need to avoid the multiple-scattering effects characteristic of the near-UV region of the spectrum. The use of wavelengths longer than about 450 nm reduces the need of accurately accounting for the multiple-Rayleigh-scattering component of the upwelling radiation and therefore facilitates the inversion process. However, as a result of interest in the study of the ozone layer during the last three decades, radiative transfer models in the ultraviolet which include molecular multiple scattering as well as particle scattering have achieved a high degree of accuracy. Therefore the need to include multiple-scattering effects is no longer a constraint in inversion algorithms. In this paper we present the theoretical basis of aerosol detection using satellite measurements of backscattered UV radiation and the method used to obtain optical depth. First, we describe how the aerosol models used in this study were selected. This is followed by a detailed discussion of the effects of these aerosols on the backscattered radiation in the near-UV (320–400 nm), where the ozone absorption is weak and does not affect the interaction between the aerosols and the molecular atmosphere. Next, we discuss alternative methods of detecting these aerosols from the measurements at two UV wavelengths (340 and 380 nm) and present the sensitivity of these methods to various error sources in estimating the aerosol optical depth. Finally, we demonstrate the application of our proposed techniques by applying it to the data taken by the TOMS instrument.

2. Aerosol Models

The atmospheric aerosol distribution exhibits large spatial and temporal variability in composition, size, and concentration related to the geographic locations of the emission sources, type of emission, diffusive transfer, and removal processes. The fluctuations of meteorological parameters (humidity, temperature, wind speed, and direction) have a direct effect on the aerosol vertical and horizontal distributions as well as on the processes of diffusion, sedimentation, and coagulation of aerosols. The optical and microphysical properties of the different types of atmospheric aerosols span a wide range of values. A theoretical analysis of all possible aerosol types is very complicated and impractical. Thus to carry out a sensitivity analysis, it is necessary to simplify the problem by selecting a set of microphysical models representative of the most commonly observed aerosol types. A brief discussion on the rationale used in the selection of the aerosol models is presented next.

2.1. Nonabsorbing Aerosols

Suspended sea-salt particles and sulfate aerosols are the most common type of nonabsorbing aerosols. Sea-salt aerosols are entirely of natural origin, whereas the sources of sulfate aerosol include both natural and anthropogenic mechanisms. Two nonabsorbing aerosol models covering two particle size ranges are used in this study. A small-particle size model (S1) representative of tropospheric sulfate aerosols of anthropogenic origin [*Shaw*, 1979] and a large-particle model (S2) representative of other nonabsorbing aerosol types such as sea-salt aerosols and stratospheric sulfuric acid aerosols [*Torres et al.*, 1995]. The refractive index of the sulfate aerosol models is prescribed on the basis of reported laboratory measurements at UV wavelengths [*Beyer et al.*, 1996]. The parameters of these aerosol models are listed in Table 1.

2.2. Carbonaceous Aerosols

Carbonaceous aerosols generated by biomass combustion consist of a mixture of material with varying radiative properties, both absorbing and nonabsorbing. Among these, the group of volatile organic or inorganic components is relatively nonabsorbing. Much of the absorption of carbonaceous particles is due to the fraction of elemental or graphitic carbon. Smoke components are produced from four fire stages: preignition, flaming, smoldering, and glowing. The relative amount of elemental carbon and, consequently, the absorption properties of the resulting smoke vary through the combustion process. Analysis of laboratory fires [*Patterson and McMahon*, 1984] as well as in situ observations [*Radke et al.*, 1991] show significantly larger absorption during the flaming combustion than during the smoldering phase of the fire. By examining the time evolution of the Angstrom coefficient of smoke aerosols, *Westphal and Toon* [1991] concluded that the size of smoke aerosol particles increases systematically, reaching geometric

mean radii between 0.10 and 0.14 μm, which is in the range of values obtained by direct particle size measurements [*Radke et al.*, 1991; *Anderson et al.*, 1996; *Remer et al.*, 1997]. As concluded by *Radke et al.* [1991], from an analysis of 17 biomass fuel fires in the temperate zone the size distribution of smoke aerosol particles show little variation from fire to fire or during a fire while near the source. The high degree of consistency of smoke aerosol size distributions was also observed by *Anderson et al.* [1996] over Brazilian and African smoke source regions during the TRACE-A experiment. The well-defined mode radius (about 0.12 μ) characteristic of the accumulation mode aerosols, which are a primary combustion product [*Radke et al.*, 1991], showed only a slight tendency to increase with smoke age, and no appreciable differences in size distribution were observed between the source areas and the outflow regions. Particle radii derived from sky spectral radiances measured by Sun/sky radiometers in Brazil also clearly shows the accumulation mode with a well-defined modal radius of 0.13 μ [*Remer et al.*, 1996].

On the basis of the documented physical nature of the evolution of biomass burning smoke optical properties, we have selected two carbonaceous aerosol models (C1 and C2). Both models have the same particle size distribution but differ in the magnitude of the imaginary component of the refractive index. The form of the assumed size distribution is a lognormal function with mode radius 0.14 μ and width 1.45. These parameters were found to adequately represent the accumulation mode of the observed size distribution over Brazilian and African sources as depicted by *Anderson et al.* [1996, Figures 4, 8, and 9]. Model C1, representative of weakly absorbing smoke aerosols away from the source area, has an imaginary refractive index of 0.02. Model C2, representative of fresh, more absorbing, smoke in the vicinity of the source area has an imaginary refractive index of 0.04. These are typical values within the range of recommended values in the visible, based on experimental work [*Patterson and McMahon*, 1984]. Measurements in the UV are not available.

2.3. Mineral Aerosols

Mineral or dust aerosol is a common type of atmospheric suspended matter characteristic of the Earth's arid and semiarid regions accounting for about one third of the planet's land surface area. Because of the high insolation levels and strong convective processes characteristic of arid regions, dust particles are easily lifted to high altitudes and horizontally transported by synoptic-scale atmospheric disturbances to areas thousands of kilometers away from their source regions [*Carlson and Prospero*, 1972]. Measurements of desert dust aerosol composition indicate a mixture of different kinds of materials with calcium, silicon (in the form of quartz), and iron (in the form of hematite), identified as the main elemental components. Although desert dust from the same source region exhibits relatively uniform physical and chemical properties over large areas, there is considerable variability in aerosol properties associated with the nature of the crustal material from different source regions [*Gomes and Gillette*, 1993].

The complex refractive index of desert dust is largely determined by the volume fraction of hematite present in the mixture. Real refractive index values of about 1.5 are generally used in the visible based on the measurements of Saharan aerosols by *Patterson et al.* [1977] at 550 and 633 nm. Measured values of the imaginary refractive index at 400 nm at a variety of locations (see survey by *Sokolik et al.* [1993]) vary from about 0.005 to about 0.02. While part of the observed variability may result from the use of different measuring techniques, these measurements also reflect the differences in composition of desert aerosols from the different regions of the world where the sampling was made [*Sokolik et al.*, 1993].

The size of desert dust aerosol particles shows significant variability over several orders of magnitude from Aitken nuclei, aerosol radii less than 0.1 μ, to ultragiant particles with radii larger than 30 μ. Since the atmospheric aerosol load over deserts is the direct result of the wind's lifting ability, the airborne particle size distribution is closely related to wind speed. Commonly used dust particle size distributions include the three-model representation for background, wind-carried dust and sandstorm conditions developed by *d'Almeida* [1987], and the wind-speed-dependent model of *Longtin et al.* [1988]. Model representations of long-range transport mineral aerosols have been developed by *Schütz* [1980].

We have selected three aerosol lognormal particle size distribution models representative of desert dust to account for the large variability in particle size: a small-particle model (D1) representative of the nucleation mode [*d'Almeida*, 1987], and two long-range transport models (D2 and D3) representative of larger particles [*Schütz*, 1980]. The complex refractive index for the three models is set to be $1.57-0.015i$, considered to be representative of the composition of Saharan dust [*Patterson et al.*, 1977]. For this analysis we have ignored the spectral dependence of the refractive index in the near UV.

2.4. Particle Shape

To calculate the scattering phase function of the aerosol particles making use of Mie theory, it has been assumed that the particles are spherical. The problem of accurately accounting for particle shape in remote sensing is twofold. First, observations are needed to determine the actual shape of the particles. When actual shapes are known, the analytical tools to represent distributions of irregularly shaped particles are not always available. For the sulfate aerosol models, the spherical assumption is easily justified since surface tension forces for liquid sulfuric acid particles resulting from the gas-to-particle transformation process tend to produce spherical shapes. Carbonaceous aerosols, on the other hand, are generally a mixture of spherical, nonspherical, and chain aggregates depending on the type of burning matter, combustion phase, and the age of the smoke. The actual shapes and sizes of combustion aerosols were measured by means of scanning electron microscopy (SEM) during the SCAR-B (Smoke, Clouds, and Radiation–Brazil) experiment. As reported by *Martins et al.* [1996], the SEM analysis showed high variability in particle shape during the flaming phase of the fire and nearly spherical particles in the smoldering phase. They also determined the asymmetry of the particles by measuring the percent change in the integrated light scattering as the particles orient themselves along an applied electric field [*Weiss et al.*, 1992]. The measured asymmetry factor during SCAR–B was always less than 11% [*Martins et al.*, 1996]. Thus on the basis of observational evidence, the representation of carbonaceous aerosols as spherical particles seems to be a reasonably good approximation. For desert dust aerosols the sphericity assumption is difficult to justify since dry aerosol particles are seldom spheres. Model calculations [*Koepke and Hess*, 1988; *Mishchenko et al.*, 1995] show that the phase function of nonspherical particles significantly deviates from that of spherical aerosols. The phase function departure from the spherical model is particle size and scat-

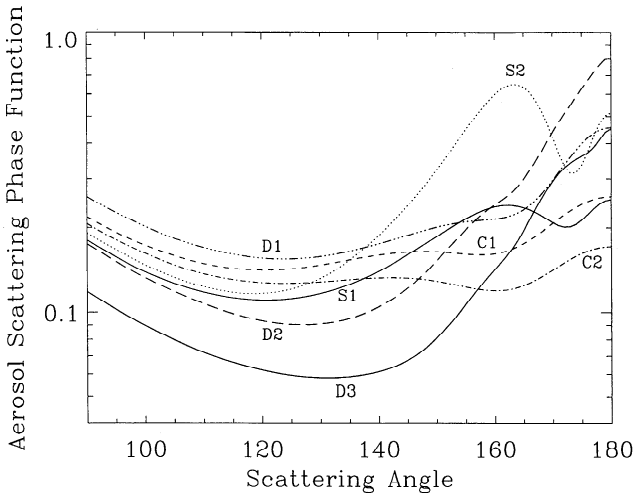

Figure 1. Scattering phase functions (at 380 nm) for the aerosol models in Table 1. The phase functions are plotted only for the range of scattering angles relevant to satellite remote sensing.

tering angle dependent with the biggest effect at scattering angles between 90° and 140° for particles of effective radii larger than about 0.5 μ. Although the particle shape is important in most of the range of scattering angles relevant to satellite remote sensing, the phase function deviation from sphericity is minimum in the range 150°–160°. Depending on the actual particle shape and viewing geometry, space retrievals of aerosol optical depth at visible wavelengths may be underestimated at backscattering geometries and overestimated at side-scattering angular configurations [*Mishchenko et al.*, 1995].

Modeling the effect of nonsphericity of aerosol particles in the near UV is required to fully assess the limitations of the spherical approximation of mineral aerosols used in this work. Because of the larger multiple-scattering contribution to the total backscattered intensity in the near UV, relative to the visible, the use of the spherical particle approximation to retrieve optical depth from measurements in the 320–400 nm range may produce smaller errors than a similar estimate in the visible region. Furthermore, the effect of particle shape on scattering properties of nonspherical particles becomes weaker with increasing imaginary component of the refractive index [*van de Hulst*, 1957]. Since the desert dust imaginary refractive index in the UV is almost an order of magnitude larger than at 630 nm, the effect on nonsphericity on the phase function may also be less important in the UV than in the visible.

These models (S1, S2, C1, C2, D1, D2, and D3) approximate the most common types of aerosols found in the Earth's atmosphere, i.e., nonabsorbing sulfate aerosols, organic carbon aerosols, and desert dust aerosols. The effect of volcanic ash aerosols is not considered in this analysis since it is only rarely present in the atmosphere. The effects of volcanic ash in the backscattered UV radiation are reported by *Krotkov et al.* [1997]. The effect of each aerosol model is considered separately; that is, no aerosol mixtures are considered. The physical properties of the above described aerosol models are summarized in Table 1. In order to have radiatively equivalent models, the optical depth at 380 nm has been set to unity for all seven models. Notice that in spite of the fact that the wavelength dependence of the refractive index in the near UV has been ignored, the computed optical thickness and single-scattering albedo are spectrally dependent due to the variation with wavelength (λ) of the aerosol size parameters, i.e., $2\pi a/\lambda$, where a is particle size. The resulting scattering phase functions for all models are depicted in Figure 1 for the range of scattering angles relevant to space measurements.

3. Effect of Aerosols on Near-Ultraviolet Radiances

The effect of aerosols in the ultraviolet radiation field has traditionally been studied in the context of ozone retrieval from space-based measurements of backscattered ultraviolet (buv) radiation. The wavelength dependence caused by absorbing and nonabsorbing aerosols on the buv radiance was first documented by *Dave* [1978] in his analysis of aerosol-related errors in the ozone retrieval from buv measurements. Additional wavelength and angular dependencies that arise from the presence of stratospheric sulfate aerosols [*Bhartia et al.*, 1993; *Torres et al.*, 1995] have been discussed. *Torres and Bhartia* [1995] considered the artifacts introduced by stratospheric aerosols on ozone profile retrieval by the SBUV family of instruments. *Torres et al.* [1995] used the strong angular dependence of the aerosol effect on the TOMS buv measurements to infer optical depth and particle size of the Mount Pinatubo aerosol layer in the tropics. *Krotkov et al.* [1997] examined the effect of volcanic ash clouds in the UV radiation field.

In this section we use radiative transfer calculations to examine the sensitivity of the buv radiance at the top of the atmosphere, to changes in the physical properties of both absorbing and nonabsorbing particles as represented by the array of aerosol model previously described. The radiative transfer model used in this study is a modified version of the Vector Program D (VPD) developed by *Dave* [1972]. It fully accounts for all orders of scattering, including the effects of polarization. Though the effect of the Earth's sphericity is taken into account for the incoming radiation, higher-order scattering is assumed to take place in a plane parallel atmosphere. Comparative analysis of this pseudospherical approximation to results using a fully spherical code [*Caudill et al.*, 1997] suggest that errors in the approximation used in the VPD code are small (<1%) at solar zenith angles less than 80°.

In addition to the aerosol models, input data on surface reflectivity, aerosol profile, and viewing geometry are required. Although the sensitivity analysis for changes in those parameters was examined, a set of baseline values of reflectivity, aerosol altitude, and solar zenith angle was selected. The wavelength-independent surface reflectivity (0.05) is based on the long-term analysis of the 380 nm minimum reflectivity measured by the Nimbus-7 TOMS instrument [*Herman and Celarier*, 1997]. The neglect of the spectral dependence agrees with the observational work of *McKenzie et al.* [1996]. The vertical distribution of mineral and carbonaceous aerosols is represented by a Gaussian profile with maximum at 3 km and a width of 1 km. This vertical distribution is assumed to be representative of an average profile since lidar measurements of both smoke and dust layers indicate that the aerosol layers typically reside between 2 and 5 km. The nonabsorbing aerosol profile is prescribed using the parameterization of *Spinhirne et al.* [1997], based on lidar observations during the Global aerosol Backscatter Experiment (GLOBE). The baseline values of solar and satellite zenith angles are 40° and 0°, respectively, corresponding to a scattering angle of 140°. Calculations at

320, 340, 360, 380, and 400 nm were conducted. A general analysis of the spectral dependence of the aerosol effect is first presented followed by a detailed account of the sensitivity of the 380 nm intensity to changes in aerosol and other related parameters.

3.1. Spectral Dependence

At wavelengths longer than 320 nm, where ozone absorption is weak, the net aerosol effect on the backscattered radiation at the top of the atmosphere is the result of the complex interaction of several competing radiative transfer processes: Rayleigh and Mie multiple scattering, aerosol absorption of both Rayleigh- and Mie-scattered radiation, as well as scattering and absorption of radiation reflected by the underlying surface. Thus the resulting backscattered radiance may increase or decrease with respect to a purely molecular atmosphere depending on the aerosol physical properties, i.e., complex refractive index, particle shape, particle size distribution, and total aerosol optical depth. In addition, the location in the atmosphere of the aerosol layer and the reflectivity of the underlying surface also affect the resulting impact of aerosols.

Even in the case of gray aerosols, i.e., aerosols with wavelength-invariant optical properties, the wavelength dependence of the backscattered radiance from an atmosphere containing aerosol particles deviates significantly from that of an aerosol-free atmosphere. The spectral dependence of the aerosol effect, presented as the percent change in backscattered radiance relative to the Rayleigh-scattering limit, is shown in Figure 2 for the seven aerosol models and two values of reflectivity of the underlying surface. In Figure 2a the transition from a radiance increase at all wavelengths for nonabsorbing aerosols to a radiance decrease for highly absorbing aerosols is due to the competing effects of aerosol scattering and absorption. Since the aerosols have a strong forward scattering, the nonabsorbing aerosols do not significantly alter the background radiation generated by molecular scattering and surface reflection but add a weakly wavelength-dependent component to the strongly wavelength-dependent molecular scattering. Therefore for such aerosols (models S1 and S2) the percent change in the radiance from the background is positive and increases with wavelength. For low values of surface reflectivity (Figure 2a) and weak to moderate aerosol absorption, aerosol scattering predominates over absorption so that there is a net increase in the amount of buv radiance at the top of the atmosphere. By contrast, highly absorbing aerosols (model D3) scatter weakly (particularly at the 140° scattering angle assumed for the plot), but they strongly absorb the background radiation. Since this absorption has only a weak spectral dependence in the near UV, there is a net, nearly wavelength-independent decrease in radiation. For higher values of surface reflectivity (Figure 2b) the effect of aerosol absorption becomes more important, while the effect of aerosol scattering at the top of the atmosphere is significantly reduced due to the enhancement of the ground reflection component that is backscattered by the aerosol layer toward the surface, where additional absorption by the surface takes place. Most aerosols therefore produce a negative change in radiance. It should be noted that because of the linearity of the aerosol effect in the near-UV illustrated in Figure 2, it is apparent that regardless of the number of measurements available, one can retrieve, at most, two pieces of information on aerosol properties.

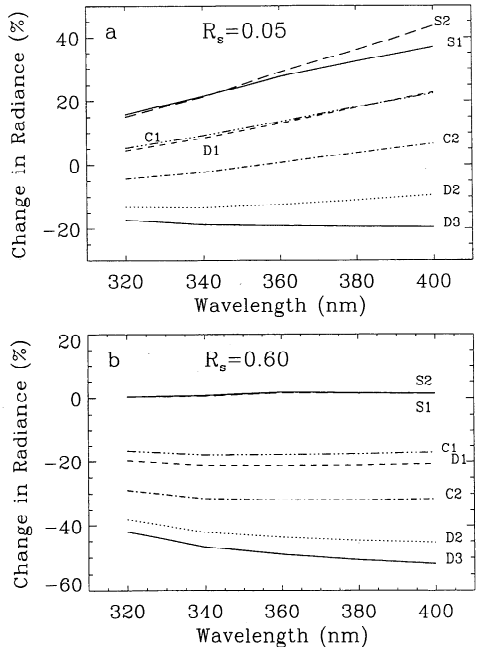

Figure 2. (a) Spectral dependence of the change in backscattered radiance, with respect to a molecular atmosphere, for the seven aerosol models used in this study (see Table 1). The results in this figure are for solar zenith angle 40° and nadir view. The reflectivity of the surface is 0.05, and the aerosol layer altitude is 2.9 km. The 380 nm optical depth is 1.0. (b) As in Figure 2a for surface reflectivity 0.6.

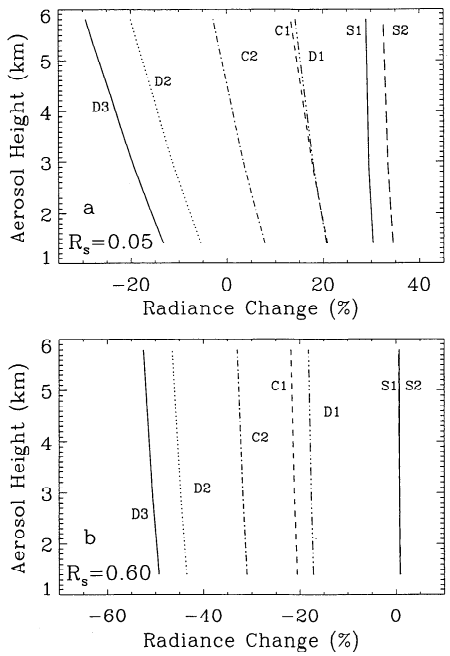

Figure 3. (a) Effect of aerosol layer altitude on the 380 nm backscattered radiance for the array of aerosol models used in this analysis. The results shown correspond to computations at three altitudes: 1.4, 2.9, and 5.8 km. Other conditions are solar zenith angle 40°, nadir view, surface reflectivity 0.05, and aerosol optical depth (380 nm) 1.0. (b) As in Figure 3a for surface reflectivity 0.6.

3.2. Effect of Aerosol Layer Height

The previous argument also explains the effect of aerosol altitude on the backscattered radiation, as shown in Figure 3

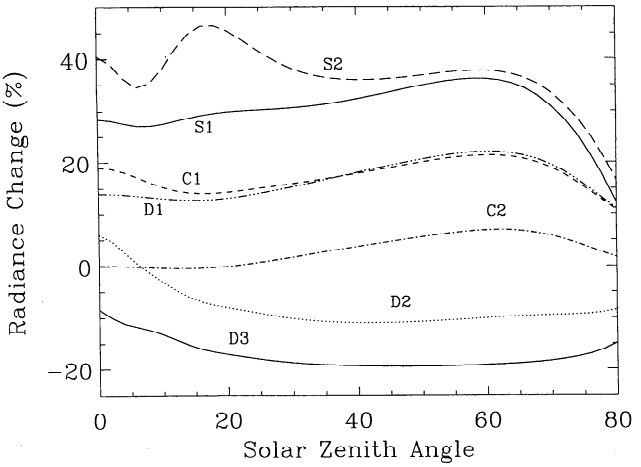

Figure 4. Angular dependence of the backscattered 380 nm radiance. Other conditions are nadir view, surface reflectivity 0.05, aerosol height 2.9 km, and aerosol optical depth (380 nm) 1.0.

for the calculations at 380 nm. For this analysis the Gaussian vertical distribution is used for the seven aerosol models. The negligible altitude dependence for models S1 and S2 supports the observation that nonabsorbing aerosols interfere little with the background radiation, whereas the increased absorption with height for model D3 at low surface reflectivity (Figure 3a) reflects the fact that these aerosols strongly absorb the molecular radiation coming from below; that is, the higher the aerosol altitude the greater the fraction of affected molecular radiation. For a bright surface beneath the aerosol layer (Figure 3b) the importance of the molecular scatter is greatly reduced, therefore the altitude dependence of the absorption effect becomes small.

3.3. Angular Dependence

The angular dependence of the aerosol effect is plotted in Figure 4 as a function of solar zenith angle. In the single-scattering approximation the percent change in backscattered radiance due to the presence of aerosols would be strictly proportional to the ratio of aerosol-to-Rayleigh scattering phase functions. For scattering angles larger than about 140° (i.e., solar zenith angles smaller than about 40°) the radiance contribution from aerosols is highly correlated with the aerosol scattering phase function. The structure of the aerosol effect in the backscatter direction is related to the glory feature present in the phase function of large particles. At larger solar zenith angles the phase function effect smears out due to the increased multiple-scattering component.

Since Figures 2 and 3 form the basis of detecting aerosols from the measurements in near UV, it is worth summarizing the findings. In near UV, aerosols produce two effects on the backscattered radiation: they produce a wavelength-dependent increase in the background radiation proportional to aerosol scattering, to which is added a wavelength-independent decrease in the radiation proportional to aerosol absorption. The former effect is independent of aerosol height, but the latter is not. It is important to note that the Rayleigh-scattering plays an important role in creating the effect; it makes the backscattered radiation highly sensitive to aerosol absorption and imparts "color" (i.e., introduces spectral dependence) to the otherwise "gray" aerosols, thus making them more easily detectable.

4. Retrieval of Aerosol Properties From Near-Ultraviolet Measurements

Remote sensing of aerosols, whether from the space or the ground, presents formidable challenges. Even for the simpler case of spherical particles, there are five aerosol parameters that affect what one measures from a remote sensing instrument: real and imaginary component of the refractive index, size distribution, particle density, and vertical distribution. Additional parameters are, of course, needed to characterize nonspherical particles. Measurements made by remote sensing instruments contain one or two independent pieces of information that simultaneously depend on several aerosol parameters. In order to derive the quantities of interest it is necessary to assume an aerosol model incorporating the other parameters. For space-based remote sensing there is the additional problem of having to know the background reflectivity accurately and of identifying cloud-free scenes. Because of the highly variable background reflectivity for wavelengths longer than 420 nm, measurements in the visible region of the spectrum have been largely restricted to the dark ocean areas.

As discussed earlier, the near-UV technique can provide at most two pieces of information about the aerosols: The spectral dependence of the change in radiances from their background values, which is proportional to aerosol scattering, and the magnitude of this change, which is proportional to aerosol absorption. The strength of the UV technique is that unlike other techniques, this information can help identify the type of aerosol that is present in a scene, thus helping one to choose the correct model for the retrieval of aerosol parameters. We have found two distinctly different ways of using the information contained in the UV radiances. Both have their strengths and weaknesses; the choice of a particular method depends on the intended application.

4.1. Residue Method

The residue method, more descriptively called the spectral contrast anomaly method, emerged as a by-product of the most recent improvement (Version 7) in the TOMS ozone retrieval algorithm [*McPeters et al.*, 1996]. As originally proposed [*Dave and Mateer*, 1967], the buv technique uses a pair of wavelengths, one ozone sensitive, the other insensitive, to derive total ozone. To do this successfully, one is required to separate accurately the spectral contrast (ratio of radiances at the selected wavelengths) caused by ozone absorption from that caused by all other effects, including molecular scattering, surface reflection, aerosols, and clouds. The Lambert-equivalent reflectivity (LER) method was proposed by *Dave and Mateer* [1967] to address this problem. In the LER method the spectral variation of buv radiances is predicted by assuming that the atmosphere consists only of molecular scatterers and absorbers (primarily ozone) bounded by a Lambertian surface. With this assumption, accurate radiative transfer calculations, including polarization and all orders of molecular scattering, are possible [*Chandrasekhar*, 1950; *Dave*, 1964]. The reflectivity of the surface is selected to be the value that predicts the measured radiances at one UV wavelength (typically 380 nm).

Although detailed radiative transfer calculations, which included the effects of aerosols and cloud scattering [*Dave*, 1978] as well as non-Lambertian surfaces [*Ahmad and Fraser*, 1982], had confirmed the theoretical validity of the LER technique for the retrieval of ozone amounts, the method was not directly validated using measurements until the development of the

TOMS V7 algorithm. Nimbus-7 TOMS had four wavelengths (331, 340, 360, 380) where the ozone absorption is weak, so the validity of the LER method to reproduce the spectral dependence of the measured radiances at these wavelengths could be directly tested. The residue r_λ, as defined in (1),

$$r_\lambda = -100[\log (I_\lambda/I_{380})_{\text{meas}} - \log (I_\lambda(\Omega, R_{380})/I_{380}(R_{380}))_{\text{calc}}], \quad (1)$$

provides a measure of the error in predicting the spectral contrast using the LER method. (It is very nearly equal to the percentage difference between the measured spectral contrast and that predicted using the LER method, divided by −2.3. The actual definition is in terms of "N values," historically used by the ground-based Dobson network, and adopted by NASA's buv team. A unit of N value is equal to 2.3% change in radiance.) In the above equation, Ω and R_{380} are the measured total ozone amount and 380 nm reflectivity, respectively.

An analysis of the residuals revealed that the LER method, though it works well in a large number of cases, does not correctly reproduce the measured spectral contrast in several notable instances. These include scenes containing broken or thin clouds, Sun glint from water, and UV-absorbing aerosols. All these effects are now well understood. Here we shall concentrate on just the aerosols.

The simulated 340 nm residues for the seven aerosol models introduced earlier are shown over both dark (Figure 5a) and bright (Figure 5b) backgrounds. Absorbing aerosols produce positive residues that increase with the aerosol optical depth, with the slope being proportional to the single-scattering albedo. Since ω_0 depends on the imaginary refractive index and the particle size distribution, variations in either of these two microphysical properties translate into a slope change in Figure 5. For low values of surface reflectivity (Figure 5a) the small-particle sulfate aerosol model (S1) yields negative residues, whereas the large particle nonabsorbing aerosol model (S2), which also mimics the behavior of thin clouds, produces almost zero residue. As illustrated in Figure 5b, absorbing aerosols are also detectable by the residue method over highly reflective surfaces. Nonabsorbing aerosols, however, are not detectable when the underlying reflective surface is bright. Other simulation results (not shown) indicate that low level (<25 km) weakly absorbing aerosols yield negative residues and cannot be distinguished from nonabsorbing aerosols. These results in Figure 5 are consistent with actual observations by *Herman et al.* [1997], who have shown that UV-absorbing aerosols, particularly smoke from biomass burning and desert dust, produce positive residues. Treating the residues as an uncalibrated aerosol index, they have been able to track these aerosols with a high degree of fidelity, identifying their sources over land and tracking them as they are transported under prevailing winds. Unpublished results show that sulfate aerosols do produce negative residues, as predicted by the S1 model, and are located in the region of high industrial activity.

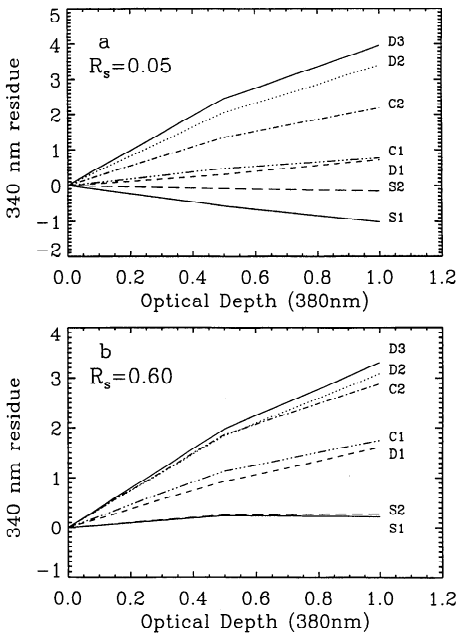

Figure 5. (a) Relationship between the aerosol index and the 380 nm optical depth for the seven aerosol models. Other conditions are solar zenith angle 40°, nadir view, surface reflectivity 0.05, and aerosol layer height 2.9 km. (b) As in Figure 5a for surface reflectivity 0.6.

Table 2. Error Analysis for Retrieval of Optical Depth Using the Residue Method

Error, %	C1	C2	D1	D2	D3
$\delta_R\tau$	±5	±1	±2	±0	±0
$\delta_Z\tau$	−10 15	−25 55	−10 15	−30 65	−40 70
$\delta_C\tau$	−10	−10	−10	−20	−20

The value $\delta_R\tau$ is the error in optical depth resulting from an uncertainty of ±0.01 in the value of surface reflectivity; $\delta_Z\tau$ is the optical depth error due to a ±1 km uncertainty in the prescribed aerosol layer altitude; $\delta_C\tau$ is the error in optical depth due 10% subpixel cloud contamination.

Qualitatively, the ability of the residue method to distinguish absorbing aerosols can be understood by noting that clouds and large sulfate particles (model S2) gives nearly zero residues, because their effects are very similar to a simple increase in surface albedo assumed by the LER model. Other types of aerosols produce wavelength dependencies that do not match those predicted by the LER model and thus produce residues.

The principal strength of the residue method is that the clouds are automatically eliminated from the data. Only the UV-absorbing aerosols are seen when the positive residues are mapped. For this type of aerosols the method works over snow/ice surfaces, or when underlying clouds are present, and even when the scene is mixed, containing absorbing aerosols and clouds. The distribution of small-particle nonabsorbing aerosols can also be observed over land and water surfaces (free of snow or ice) when the negative residues are mapped. However, large-particle nonabsorbing aerosols (model S2) are not detectable, and small amounts of weakly absorbing aerosols (models S1, C1, and D1) are harder to detect over the instrument noise (roughly ~0.2 N units).

The principal limitation of the residue method is that one needs to know which aerosol model to use in order to derive the optical thickness. Selection of a wrong model can give errors of a factor of 4 or more. The errors in derived optical depth due to the uncertainty on the prescribed surface reflectivity, aerosol layer altitude, as well as the effect of subpixel cloud contamination for the different aerosol types (it has been assumed that the aerosol type is known) are shown in Table 2. The residue method is largely insensitive to errors in surface

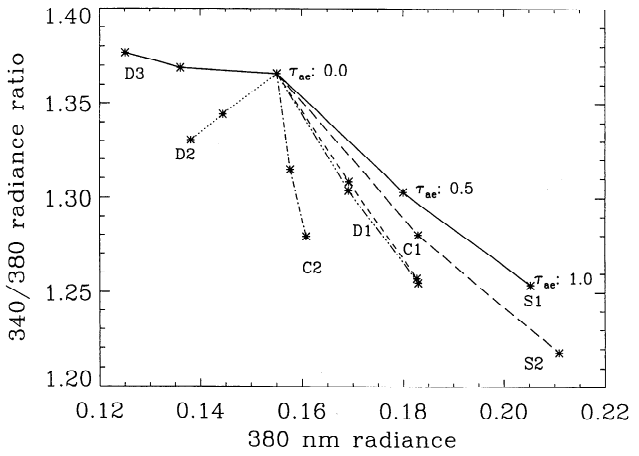

Figure 6. Ratio of the backscattered radiance at 340–380 nm as a function of 380 nm radiance for the aerosol models assumed in this work. Symbols represent calculations at aerosol optical depth values of 0, 0.5, and 1.0. Other conditions as in Figure 5.

reflectivity. The error in optical depth due to uncertainty of the surface reflectivity is proportional to the aerosol amount, yielding maximum optical depth error of 5% for weakly absorbing aerosols. As the aerosol absorption increases, the resulting error becomes negligible. Errors as large as 70% may result due to the uncertainty in aerosol height which must be known rather precisely, particularly for highly absorbing aerosols. The optical depth is underestimated (overestimated) when the prescribed location of the aerosol layer is higher (lower) than the actual aerosol location. Notice that altitude underestimation yields larger optical depth errors than altitude overestimation. Subpixel cloud contamination effects were evaluated by linearly combining cloud- (10%) and aerosol- (90%) generated backscattered radiances. From Table 2, one also notes a unique feature of the residue method: it correctly underestimates the optical thickness when the aerosols are obscured by subpixel clouds, even though the clouds themselves are much brighter than the aerosols. Most other methods would overestimate the aerosols by a large amount. However, the residue method overcorrects highly absorbing aerosols, because of nonlinearities in the algorithm.

Verification of the TOMS aerosol detection capability by this method has been discussed in terms of distribution and frequency of occurrence [*Herman et al.*, 1997; *Hsu et al.*, 1996; *Seftor et al.*, 1997] by comparison with ground-based Sun photometer data and AVHRR satellite data. Since results of the application of the residue method to map the global distribution of absorbing aerosols have been adequately covered elsewhere, we do no include them here.

4.2. Direct Method

The relationship between the 340/380 nm radiance ratio and the 380 nm radiance constitutes the basis of a direct way of determining aerosol properties taking advantage of the spectral contrast change (with respect to a molecular atmosphere) which is measured from space, when the atmosphere contains aerosols. Such a relationship is depicted in Figure 6 for the set of aerosol models adopted for this analysis. It is clear that at least within the domain of these models, one can identify the different aerosol types or mixtures thereof (except for differentiating between the C1 and the D1 models whose radiative effects are very similar). Thus in addition to the aerosol optical depth the direct method produces a measurement of the absorptivity of the aerosol which may also be interpreted as an effective single-scattering albedo. As shown in Figure 6, large-particle nonabsorbing aerosols may be hard to separate from some types of weakly absorbing ones. The effect of this ambiguity may be reduced by using the sign of the 340 nm residue as a qualitative indicator of the type of aerosol present to select the most appropriate set of aerosol models for the retrieval. For the nonabsorbing aerosols the remaining piece of information can be used to infer the aerosol-effective particle size. Unlike the residue technique, the direct method is sensitive to all aerosol types, including weakly absorbing and large-particle nonabsorbing aerosols. Sensitivity analysis results (not shown) indicate that this method can be applied to scenes with near-UV surface reflectivity as high as 0.2. Since in this spectral range the reflectivity of all land- and ocean-covered areas (in the absence of ice and snow) is well below 0.2 [*McKenzie et al.*, 1996; *Herman and Celarier*, 1997], this method can be applied over most regions of the Earth under cloud-free conditions.

Under cloud-free conditions the accuracy of the retrieved quantities is determined mainly from the errors in the prescribed surface reflectivity and aerosol layer height. A summary of the errors in optical depth due the uncertainty in surface reflectivity and aerosol layer altitude is presented in Table 3. For a surface reflectivity uncertainty of ± 0.01 the accuracy of retrieved optical depth is ± 0.1 for nonabsorbing and weakly absorbing aerosols. As the aerosol becomes more absorbing, the reflectivity of the surface is less important, and the accuracy of the retrieval is better than ± 0.05. Although this error may be significant in percent terms for small values of optical depth, it represents only a small error for an optically thick smoke or dust aerosol layer. The surface effect, however, determines the minimum retrievable optical depth which we estimate to be about 0.2 ± 0.1. The effect of ± 1 km uncertainty in the prescribed aerosol height on the accuracy of the retrieved optical depth is also quantified in Table 3. Negligible optical depth errors ($\pm 2\%$) result for nonabsorbing aerosols. However, as aerosol absorption increases, so does the altitude error in optical depth which may be larger than 60% for

Table 3. Error Analysis for Retrieval of Optical Depth Using the Direct Method

Error	S1	S2	C1	C2	D1	D2	D3
$\delta_R\tau$	± 0.10	± 0.10	± 0.10	± 0.10	± 0.10	± 0.05	± 0.02
$\delta_Z\tau$, %	-2 2	-2 2	-5 9	-18 45	-5 10	-25 60	-35 65
$\delta_C\tau$, %	20	20	20	25	20	30	40

The value $\delta_R\tau$ is the absolute error in optical depth resulting from an uncertainty of ± 0.01 in the value of surface reflectivity; $\delta_Z\tau$ and $\delta_C\tau$ are the percent errors in optical depth due to uncertainty in aerosol altitude and cloud contamination as in Table 2.

strongly absorbing aerosols. As with the residue method, the error is larger (optical depth is overestimated) when the aerosol height is underestimated than when it is overestimated by the same distance (optical depth is underestimated). Another important source of error included in Table 3 is the presence of subpixel clouds which causes an overestimation of the optical depth. Backscattered radiances affected by 10% cloud contamination yield optical depth errors between 20% and 40% depending on the type of aerosol present.

The error analysis of the retrieved effective single-scattering albedo is shown in Table 4. When the surface reflectivity is prescribed within 0.01, the accuracy of the effective ω_0 goes from 0.004 for weakly absorbing aerosols to 0.03 for strongly absorbing particles. By the same token, if the prescribed height of the aerosol layer is accurate within 1 km, the ω_0 error goes from 0.01 to 0.04 as aerosol absorption increases. By far, the most important source of error in effective ω_0 is cloud contamination. As shown in Table 4, a 10% subpixel cloud contamination causes an ω_0 overestimation of about 0.15.

The direct method has been applied to measurements of backscattered UV radiation by the TOMS instrument which measures the buv radiance at six wavelengths. Data from four different TOMS sensors are available. The TOMS instruments onboard the Nimbus-7 spacecraft (1979–1993) and on the Russian Meteor-3 satellite (1991–1994) measured buv radiances at 313, 318, 331, 340, 360, and 380 nm. Two more TOMS sensors, on the Earth probe and ADEOS platforms started operation during the summer of 1996. An example of the application of the direct method to the Nimbus-7 TOMS data is shown in Plates 1 and 2. To minimize the problem of cloud contamination, all scenes for which the 340 nm residue is less than 0.2 are eliminated. Along with clouds this screening process also removes large-particle sulfate aerosols and weakly absorbing aerosols and may not completely eliminate mixed scenes containing strongly absorbing aerosols and subpixel clouds. In addition, scenes over water within the Sun glint viewing geometry and scenes with reflectivity greater than 0.15 are also eliminated. The use of a reflectivity threshold helps to screen out bright clouds and snow-ice-covered surfaces. For the remaining scenes we apply the direct method to compute the optical depth, by assuming, for this example, that the aerosol layer is 2.9 km above sea level. The values of surface reflectivity used in the calculation are obtained from a climatology of minimum 380 nm TOMS reflectivity, based on the statistical analysis of *Herman and Celarier* [1997], with an additional screening on the 340 nm residue to ensure that only data with minimum aerosol contamination are used. This approach reduces the effect of strongly absorbing aerosols that might make the underlying surface appear darker than it is actually.

Plate 1 provides a 1 day global map of the 380 nm aerosol optical depth of absorbing aerosols for September 10, 1981, over both land and water surfaces. Large plumes of carbonaceous and mineral aerosols are clearly observed over both the source regions and over the oceans as the aerosols are transported over long distances by the prevailings winds. The geographical distribution of optical depth on this day clearly shows large aerosol concentrations over the smoke source regions of Brazil and southern Africa. The large values over the Sahara Desert and off the western shore of northern Africa are associated with the dust outbreaks known to take place in this area at this time of the year. Plate 2 shows a distribution of the effective single-scattering albedo associated with the aerosol model combination selected by the direct method.

Table 4. Error Analysis for Retrieval of the Effective Single-Scattering Albedo

Error	C1	C2	D1	D2	D3
$\delta_R\omega_0$	±0.004	±0.006	±0.002	±0.018	±0.030
$\delta_Z\omega_0$	±0.012	±0.015	±0.010	±0.025	±0.040
$\delta_C\omega_0$	0.015	0.02	0.010	0.10	0.15

The values $\delta_R\omega_0$ and $\delta_Z\omega_0$ are the resulting absolute errors due to uncertainties in the prescribed values of surface reflectivity (±0.01) and aerosol layer height (±1 km); $\delta_C\omega_0$ is the error in single-scattering albedo due to 10% of subpixel cloud contamination.

A preliminary evaluation of the accuracy of the direct method to retrieve optical depth was carried out by comparing satellite-derived optical depth to ground-based Sun photometer measurements. Figure 7 shows a comparison of optical depths derived from backscattered radiances measured by the GOME and TOMS sensors, to ground-based measurements at sites in Brazil during the SCAR-B experiment in 1995 [*Gleason et al.*, 1998], and Africa in 1986, 1987, and 1992 (D. Tanre, personal communication, 1997). The SCAR-B events correspond to smoke aerosols, whereas the African data are primarily measurements of Saharan dust. To make the comparison meaningful, when necessary, the satellite-derived values at 380 nm were converted to the Sun photometer wavelength using Mie theory. The error bars (±30%) are our estimates of the uncertainty on the retrieved optical depth due to the combined effect of cloud contamination and errors in the prescribed values of surface reflectivity and aerosol layer height. The observed level of agreement indicates that for most of these comparisons the assumption about the altitude of the aerosol layer (2.9 km) is not too far from reality. The results of these comparisons are encouraging, given the differences in sampling point measurement at the ground versus 10^4 square kilometer area average from the satellite measurements. A more detailed validation analysis of satellite-derived optical depth using the BUV technique will be published separately.

5. Summary and Concluding Remarks

We have discussed the basis of a new method to detect and characterize aerosols using the strong wavelength dependence of backscattered radiance in the near ultraviolet. The techniques presented here are particularly useful to retrieve information on absorbing aerosols. The residue method is a useful way of separately mapping the spatial distribution of UV-absorbing and small-size nonabsorbing particles without the clouds showing up in the map. Absorbing aerosols are detected over any terrestrial surface, including snow/ice or above clouds, whereas the nonabsorbing aerosols are detectable over both land and water surfaces but not over highly reflecting surfaces such as snow/ice or clouds. This method, however, cannot be used to make quantitative estimates of the optical thickness, unless there is external information about the type and altitude of aerosol present at particular geographic locations. The direct method, on the other hand, can be used to derive aerosol optical thickness and an effective single-scattering albedo over cloud- and ice-/snow-free scenes, provided the height of the aerosol layer and reflectivity of the surface are known or prescribed.

The main shortcomings in the application of the direct method are the presence of subpixel clouds and the uncertainty on the height of the aerosol layer. For the TOMS instruments, neither of these obstacles can be overcome without the use of

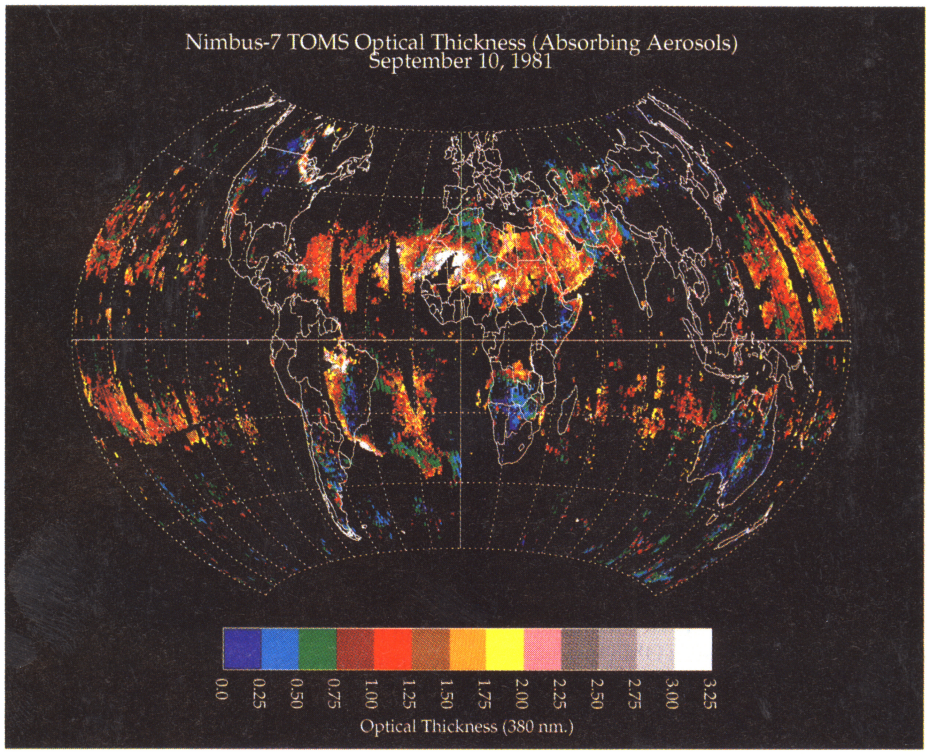

Plate 1. Map of retrieved 380 nm optical depth on September 10, 1981.

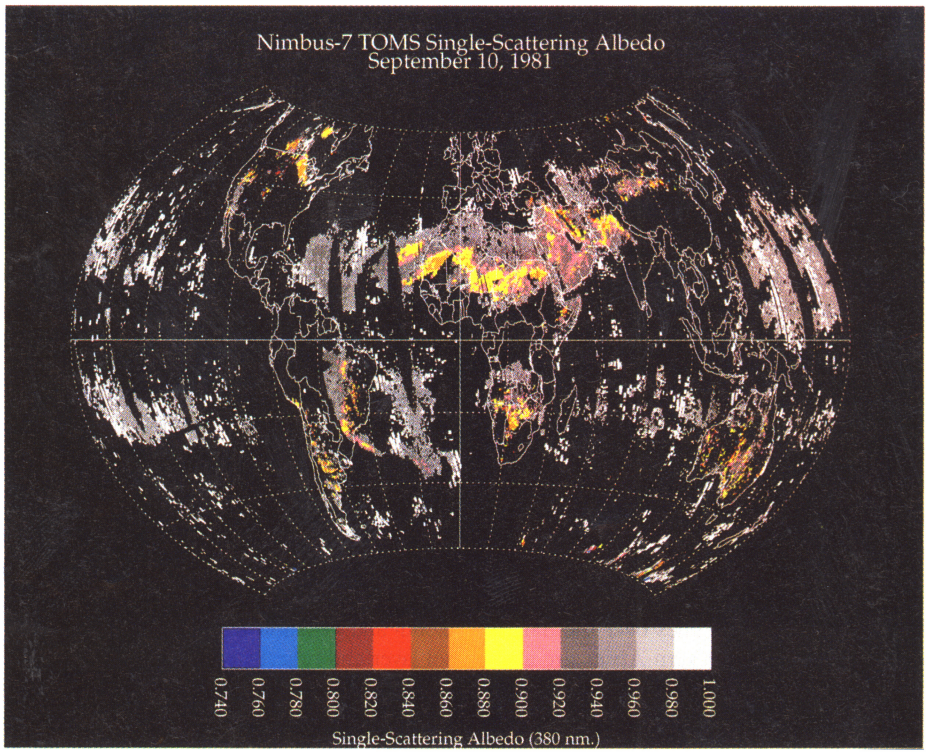

Plate 2. Map of the distribution of effective single-scattering albedo on September 10, 1981.

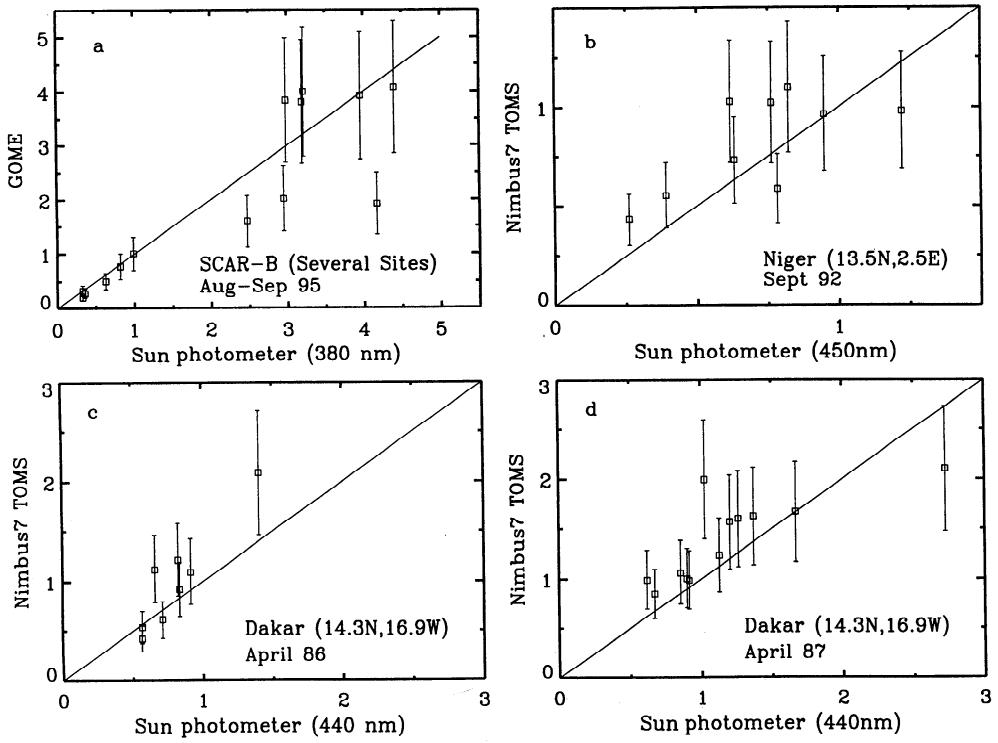

Figure 7. Comparison of optical depth derived from satellite measurement of buv radiances to collocated Sun photometer measurements. Smoke optical depth during SCAR-B were derived using (a) GOME-measured radiances. Dust optical depth over (b) Niger and (c and d) Dakar were retrieved from Nimbus 7/TOMS data.

external information. Given the large TOMS footprint, subpixel cloud contamination is by far the largest problem. The use of a reflectivity threshold helps to eliminate the obvious cloud contamination cases, but optically thin clouds may not be screened out with this technique. The problem of aerosol layer altitude may be addressed with the use of a climatological database compiled from space and airborne lidar measurement of aerosol backscatter profiles over the main biomass burning regions of the world and mineral aerosol sources. Several currently available (LITE, TRACE-A, ABLE, SCAR-B, ACE2) lidar data sets can be used for this purpose. Parcel trajectory modeling of observed aerosol motions can be used to determine the plume height relative to known wind shear regions for specific cases. Another possible way of determining the aerosol layer location is the use of the rotational Raman-scattering signal [*Joiner et al.*, 1995].

As it has been shown in this work, the detection capability for absorbing aerosols is enhanced in the near ultraviolet since the absorbing suspended matter acts not only on the Mie-scattered radiation but also on the Rayleigh component. As a result, the strong molecular scattering in the ultraviolet becomes an advantage since it effectively acts to create a spectral signal against the Rayleigh background when absorbing aerosols are present. Because of these unique advantages it is recommended that in the planning of future aerosol sensing experiments, the choice of wavelengths be expanded to include the 330–390 nm range to aid in the detection and characterization of absorbing aerosols.

Acknowledgments. The authors would like to thank Didier Tanre and the Laboratoire d'Optique Atmosphérique for providing the Sun photometer measurements over Africa used in this work, and the European Space Agency (ESA) for providing the GOME data used in the comparison to ground measurements in Brazil. We also thank Dave Larko for his assistance with the color graphics and two anonymous referees for their valuable comments and suggestions.

References

Ahmad, Z., and R. S. Fraser, An iterative radiative transfer code for ocean-atmosphere systems, *J. Atmos. Sci.*, *39*, 656–665, 1982.

Anderson, B. E., W. B. Grant, G. L. Gregory, E. V. Browell, J. E. Collins, G. W. Sachse, D. R. Bagwell, C. H. Hudgins, D. R. Blake, and N. J. Blake, Aerosols from biomass burning over the tropical South Atlantic region: Distribution and impacts, *J. Geophys. Res.*, *101*, 24,117–24,137, 1996.

Beyer, K. D., A. R. Ravishankara, and E. R. Lovejoy, Measurements of UV refractive indices and densities of H_2SO_4/H_2O and $H_2SO_4/HNO_3/H_2O$ solutions, *J. Geophys. Res.*, *101*, 14,519–14,524, 1996.

Bhartia, P. K., J. R. Herman, R. D. McPeters, and O. Torres, Effect of Mount Pinatubo aerosols on total ozone measurements from backscatter ultraviolet (BUV) experiments, *J. Geophys. Res.*, *98*, 18,547–18,554, 1993.

Carlson, T. N., and J. M. Prospero, The large-scale movement of Saharan air outbreaks over the northern equatorial Atlantic, *J. Appl. Meteorol.*, *11*, 283–297, 1972.

Caudill, T. R., D. E. Flittner, B. M. Herman, O. Torres, and R. D. McPeters, Evaluation of the pseudo-spherical approximation for backscattered ultraviolet radiances and ozone retrieval, *J. Geophys. Res.*, *102*, 3881–3890, 1997.

Chandrasekhar, S., *Radiative Transfer*, Clarendon, Oxford, England, 1950.

Charlson, R. J., J. Langner, H. Rodhe, C. B. Leovy, and S. G. Warren, Perturbation of the northern hemisphere radiative balance by backscattering from anthropogenic sulfate aerosols, *Tellus*, *Ser. AB*, *43*, 152–163, 1991.

d'Almeida, G. A., On the variability of deser dust radiative characteristics, *J. Geophys. Res.*, *92*, 3017–3026, 1987.

Dave, J. V., Meaning of successive iteration of the auxiliary equation in the theory of radiative transfer, *Astrophys. J.*, *140*, 1292–1303, 1964.

Dave, J. V., Development of programs for computing characteristics of ultraviolet radiation, technical report, Vector Case, IBM Corp., Fed. Syst. Div., Gaithersburg, Md., 1972.

Dave, J. V., Effect of aerosols on the estimation of total ozone in an atmospheric column from the measurements of its ultraviolet radiance, *J. Atmos. Sci.*, *35*, 899–911, 1978.

Dave, J. V., and C. L. Mateer, A preliminary study on the possibility of estimating total atmospheric ozone from satellite measurements, *J. Atmos. Sci.*, *24*, 414–427, 1967.

Gleason, J. F., N. C. Hsu, and O. Torres, Biomass burning smoke measured using backscattered ultraviolet radiation: SCAR-B and Brazilian smoke interannual variability, *J. Geophys. Res.*, in press, 1998.

Gomes, L., and D. A. Gillette, A comparison of characteristics of aerosol from dust storms in Central Asia with soil-derived dust from other regions, *Atmos. Environ.*, *27*(A), 2539–2544, 1993.

Herman, J. R., and E. Celarier, Earth's surface reflectivity climatology at 340–380 nm from TOMS data, *J. Geophys. Res.*, *102*, 28,003–28,012, 1997.

Herman, J. R., P. K. Bhartia, O. Torres, N. C. Hsu, C. J. Seftor, and E. Celarier, Global distribution of UV-absorbing aerosols from Nimbus 7/TOMS data, *J. Geophys. Res.*, *102*, 16,911–16,922, 1997.

Hsu, N. C., J. R. Herman, P. K. Bhartia, C. J. Seftor, O. Torres, A. M. Thompson, J. F. Gleason, T. F. Eck, and B. N. Holben, Detection of biomass burning smoke from TOMS measurements, *Geophys. Res. Lett.*, *23*, 745–748, 1996.

Joiner, J., P. K. Bhartia, R. P. Cebula, E. Hilsenrath, and R. D. McPeters, Rotational Raman scattering (Ring effect) in satellite backscatter ultraviolet measurements, *Appl. Opt.*, *34*, 4513–4525, 1995.

Koepke, P., and M. Hess, Scattering functions of tropospheric aerosols: The effects of nonspherical particles, *Appl. Opt.*, *27*, 2422–2430, 1988.

Krotkov, N. A., A. J. Krueger, and P. K. Bhartia, Ultraviolet optical model of volcanic clouds for remote sensing of ash and sulfur dioxide, *J. Geophys. Res.*, *102*, 21,891–21,904, 1997.

Longtin, D. R., E. P. Shettle, J. R. Hummel, and J. D. Pryce, A wind dependent desert aerosol model: Radiative properties, *AFGL-TR-88-0112*, Air Force Geophys. Lab., Bedford, Mass., 1988.

Martins, J. V., P. V. Hobbs, R. E. Weiss, and P. Artaxo, *Shapes of Smoke Particles From Biomass Burning in Brazil*, SCAR-B Proceedings, edited by V.W.J.H. Kirchhoff, Transtec Ed., São Paulo, Brazil, 1996.

McKenzie, R. L., M. Kotkamp, and W. Ireland, Upwelling UV spectral irradiances and surface albedo measurements at Lauder, New Zealand, *Geophys. Res. Lett.*, *23*, 1757–1760, 1996.

McPeters, R. D., et al., Nimbus 7 total ozone mapping spectrometer (TOMS) data products user's guide, *NASA Ref. Publ. 1384*, 1996.

Mishchenko, M. I., A. A. Lacis, B. E. Carlson, and L. D. Travis, Nonsphericity of dust-like tropospheric aerosols: Implications for aerosol remote sensing and climate modeling, *Geophys. Res. Lett.*, *22*, 1077–1080, 1995.

Patterson, E. M., and C. K. McMahon, Absorption characteristics of forest fire particulate matter, *Atmos. Environ.*, *18*, 2541–2551, 1984.

Patterson, E. M., D. A. Gillette, and B. Stockton, Complex index of refraction between 300 and 700 nm for Saharan aerosols, *J. Geophys. Res.*, *82*, 3153–3160, 1977.

Radke, L. F., D. A. Hegg, P. V. Hobbs, J. D. Nance, J. H. Lyons, K. K. Laursen, R. E. Weiss, P. J. Riggan, and D. E. Ward, Particulate and trace gas emissions from large biomass fires in North America, in *Global Biomass Burning: Atmospheric, Climatic, and Biospheric Implications*, edited by J. S. Levine, chap. 28, pp. 209–224, MIT Press, Cambridge, Mass., 1991.

Remer, L. A., Y. J. Kaufman, and B. N. Holben, The size distribution of ambient aerosol particles: Smoke vs urban/industrial aerosol, in *Biomass Burning and Global Change*, edited by J. S. Levine, pp. 519–530, MIT Press, Cambridge, Mass., 1996.

Schütz, L., Long-range transport of desert dust with special emphasis on the Sahara, *Ann. N. Y. Acad. Sci.*, *338*, 515–532, 1980.

Shaw, G. E., Considerations on the origin and properties of the Antarctic aerosol, *Rev. Geophys.*, *8*, 1983–1998, 1979.

Seftor, C. J., N. C. Hsu, J. R. Herman, P. K. Bhartia, O. Torres, W. I. Rose, D. J. Schneider, and N. Krotkov, Detection of volcanic ash clouds from Nimbus-7/total ozone mapping spectrometer, *J. Geophys. Res.*, *102*, 16,749–16,759, 1997.

Sokolik, I., A. Andronova, and T. C. Johnson, Complex refractive index of atmospheric dust aerosols, *Atmos. Environ.*, *27*(A), 2495–2502, 1993.

Spinhirne, J. D., S. Chudamani, and A. D. Clarke, Distribution of aerosol scattering throughout the Pacific basin regions from observations, in *Proceedings at the Ninth Conference on Atmospheric Radiation*, Am. Meteorol. Soc., Boston, Mass., 1997.

Tegen, I., A. A. Lacis, and I. Fung, The influence on climate forcing of mineral aerosols from disturbed soils, *Nature*, *380*, 419–422, 1996.

Torres, O., and P. K. Bhartia, Effect of stratospheric aerosol on ozone profile from buv measurements, *Geophys. Res. Lett.*, *22*, 235–238, 1995.

Torres, O., J. R. Herman, P. K. Bhartia, and Z. Ahmad, Properties of Mount Pinatubo aerosols as derived from Nimbus 7 total ozone mapping spectrometer measurements, *J. Geophys. Res.*, *100*, 14,043–14,055, 1995.

van de Hulst, H. C., *Light Scattering by Small Particles*, 470 pp., John Wiley, New York, 1957.

Weiss, R. E., V. N. Kapustin, and P. V. Hobbs, Chain-aggregate aerosols in smoke from the Kuwait oil fires, *J. Geophys. Res.*, *97*, 14,527–14,531, 1992.

Westphal, D. L., and O. B. Toon, Simulations of microphysical, radiative, and dynamical processes in a continental-scale forest fire smoke plume, *J. Geophys. Res.*, *96*, 22,379–22,400, 1991.

Z. Ahmad, Science and Data Systems Inc., Silver Spring, MD, 20906.

P. K. Bhartia, J. Gleason, and J. R. Herman, NASA Goddard Space Flight Center, Code 916, Greenbelt, MD, 20771.

O. Torres, Hughes STX Corporation, 4400 Forbes Blvd, Lanham, MD, 20706. (e-mail: torres@qhearts.gsfc.nasa.gov)

(Received July 22, 1997; revised January 14, 1998; accepted March 3, 1998.)